Cosmic star formation rate: a theoretical approach

L. Vincoletto[1]⋆ F. Matteucci[1,2] F. Calura[3] L. Silva[2] G. Granato[2]

[1] *Dipartimento di Fisica - Sezione di Astronomia - Università degli Studi di Trieste - Piazzale Europa, 1, I-34127 Trieste, Italy*
[2] *INAF - Osservatorio Astronomico di Trieste, Via G.B. Tiepolo 11, I-34131 Trieste, Italy*
[3] *INAF - Osservatorio Astronomico di Bologna, Via Ranzani 1, I-40127 Bologna, Italy*

ABSTRACT
The cosmic star formation rate (CSFR), namely the star formation rate in a unitary comoving volume of the Universe, is an important clue to investigate the history of the assembly and evolution of galaxies. Here, we develop a method to study the CSFR from a purely theoretical point of view. Starting from detailed models of chemical evolution, which best fit the properties of local galaxies, we obtain the histories of star formation of galaxies of different morphological types (ellipticals, spirals, irregulars). These histories are then used to determine the luminosity functions of the same galaxies by means of a spectro-photometric code. We obtain the CSFR under different hypotheses about galaxy formation scenarios. First, we study the hypothesis of a pure luminosity evolution scenario, in which all galaxies are supposed to form at the same redshift and then evolve only in luminosity without any merging or interaction. Then we consider scenarios in which the number density or the slope of the luminosity functions are assumed to vary with redshift. After comparison of our results with the data available in literature, we conclude that a pure luminosity evolution does not provide a good fit to the data, especially at very high redshift, although many uncertainties are still present in the data because of the unknown dust corrections and assumed initial mass function. On the other hand, a variation in the number density of ellipticals and spirals as a function of redshift can provide a better fit to the observed CSFR. We critically discuss the possible scenarios for galaxy formation derived from this finding. We also explore cases of variable slope of the luminosity functions with redshift as well as variations of number density and slope at the same time. We cannot find any of those cases which can fit the data as well as the solely number density variation. Finally, we compute the evolution of the average cosmic metallicity in galaxies with redshift and show that in the pure luminosity evolution case the ellipticals dominate the metal production in the Universe, whereas in the case of number density evolution are the spirals the main producers of metals.

Key words: galaxies: evolution - galaxies: fundamental parameters - galaxies: photometry - galaxies: luminosity function - ISM: general - ISM: evolution.

1 INTRODUCTION

The rate at which galaxies have formed stars throughout the whole cosmic time is a fundamental clue to investigate the history of the assembling and evolution of structures in the Universe. The cosmic star formation rate (CSFR), defined as the comoving space density of the global star formation rate in a unitary volume of the Universe, is not a directly measurable quantity. It can be inferred only from the measurement of the luminosity density in different wavebands, which are then transformed into star formation rate by suitable calibrations. Starting from its first determination made

by Lilly et al. (1996) and thanks to deeper and deeper surveys it has been possible to extend the determination of the cosmic star formation rate up to $z \sim 10$ (Madau et al. 1998; Hopkins 2004; Bouwens et al. 2008; Li 2008; Kistler et al. 2009; Bouwens et al. 2011a; Ishida et al. 2011). Constraining the CSFR at high redshift would be of paramount importance to put constraints in the galaxy formation scenario. In particular, to decide between the *Monolithic Collapse* (MC) and the *Hierarchical Clustering* (HC), because the CSFR depends on both the star formation rate (SFR) in galaxies and on the evolution of the galaxy luminosity function (LF). In the MC scenario, spheroids and bulges formed at high redshift (e.g. $z > 2 - 3$) as the result of a violent burst of star formation, following the collapse of a gas cloud. After the

⋆ E-mail: vincoletto@oats.inaf.it

development of a galactic wind quenching star formation, galaxies evolved passively until present time (Larson 1974; Matteucci & Tornambé 1987). Moreover, Matteucci (1994) introduced in this scenario the assumption that more massive spheroids had higher star formation efficiencies than less massive ones, and stopped to form stars earlier. It is common now to refer to this behaviour as "downsizing in star formation". These assumptions allow us to reproduce the majority of chemical and photometric properties of local ellipticals. On the other hand, in the HC scenario for galaxy formation, baryon assembly basically mirrors the hierarchical build up of dark matter structures. Therefore, spheroids and bulges formed as a series of subsequential mergers among gas-rich galaxies or with galaxies that have already stopped their star formation. In this scenario, galaxies form stars at lower rates than in the MC scenario, with more massive spheroids reaching their final mass at later times ($z \lesssim 1.5$) (White & Rees 1978; Baugh et al. 1998; Cole et al. 2000; Menci et al. 2004). In this paper, we calculate the evolution of the CSFR and the mean metallicity of the interstellar medium (ISM) in galaxies. This is done by means of detailed chemical evolution models for galaxies of different morphological types, i.e., ellipticals, spirals, and irregulars, which successfully reproduce the local properties of such galaxies, and from which we derive their star formation histories (SFH). Star formation histories obtained with chemical evolution models are then used to determine the photometric evolution of the galaxies (spectra and magnitudes), through a spectro-photometric code. This allows us to compute the LF, that gives the number of galaxies in a unitary volume of the Universe in a luminosity bin. In this work, we normalize our LFs to the local LFs derived by Marzke et al. (1998), which are based on the *"Second Southern Sky Redshift Survey" (SSRS2)* using data from 5404 galaxies at $z \leqslant 0.05$. These LFs are determined in the B band for galaxies of different morphological type. Then we compute the evolution in luminosity of the galaxy at the break of the LF for each galactic type. This is done under different scenarios: first, we study the hypothesis of a pure luminosity evolution scenario (PLE). In this case, galaxies are supposed to form all at the same redshift and then evolve only in luminosity without any merging or interaction. In this case, we follow the approach of Calura & Matteucci (2003). Then we define two new scenarios: one in which the number density of the LF is assumed to vary with redshift, and one in which the slope of the LF is assumed to vary with redshift. All the results have been compared with the available data found in literature. Finally, we calculate the mean metallicity of the ISM for the PLE and the number density evolution (NDE) scenario. The paper is organized as follows: in § 2 we describe the chemical and photometric models, in § 3 we present our results and in § 4 we draw some conclusions.

Throughout this paper the cosmology adopted will follow the ΛCDM paradigm with $\Omega_0 = 0.3$, $\Omega_\Lambda = 0.7$ and $h = 0.65$.

2   CHEMICAL AND PHOTOMETRIC EVOLUTION OF GALAXIES

Chemical evolution models allow us to compute the evolution in time and space of several quantities such as the star formation, the production rate of chemical elements and the chemical abundances in the stars and in the gas, starting from the matter reprocessed by the stars and restored into the ISM through stellar winds and supernova explosions. Starting from observational constraints such as the present day chemical abundances, it is possible to perform a detailed backward evolution of galaxies of different morphological type. We consider three galactic types namely irregulars, spiral disks and spheroids which include both bulges and elliptical galaxies. This is motivated by the fact that ellipticals and bulges are likely to have a common origin, i.e. both are likely to have formed their stars on very short timescales and a long time ago (Jablonka et al. 1996). Detailed descriptions of the adopted models can be found in Matteucci & Francois (1989) for spirals, Pipino & Matteucci (2004) for ellipticals and Bradamante et al. (1998) for irregulars.

In our picture, spheroids form as the result of a sudden collapse of a gas cloud of primordial chemical composition. The gas is supposed to be accreted over a finite timescale, so in this respect we do not assume pure MC models. A galaxy can be modelled either as a one-zone object or a multi-zone object in which the galaxy is divided into several concentric shells independent of each-other. The spheroids are modelled as a one zone objects and they are supposed to suffer a strong initial burst of star formation, that stops as soon as the galactic wind develops; in this sense their evolution crucially depends on the time at which the galactic wind occurs. From that moment on the galaxy is supposed to evolve passively.

The chemical evolution of spiral disks is studied by using the one-infall model of Matteucci & Francois (1989), developed to reproduce the observational constraints of the Milky Way disk. This model belongs to the class of the so-called *"infall models"*, where the disk is thought as gradually forming by infall of primordial gas. Instantaneous mixing of gas is assumed, but the instantaneous recycling approximation is relaxed. The galactic disk is supposed to have formed on timescales increasing with the galactocentric distance, being larger at larger radii, in agreement with the dissipative models of galaxy formation of Larson (1976). The gas accumulates faster in the inner than in the outer region, according to the so-called *"inside-out"* scenario. The process of disk formation is much longer than the halo and the bulge formation (they should form on timescales no longer than 1 Gyr) with typical timescales varying from $\sim$ 2 Gyr in the inner disk, $\sim$ 7 Gyr in the solar region and up to $15 - 20$ Gyr in the outer disk. This mechanism is important to reproduce the observed abundance gradients (see Matteucci & Francois 1989, Chiappini et al. 2001). The spiral disk is approximated by several independent rings, 2 kpc wide, without exchange of matter between them. In this work the disk has been set to extend from 2 to 16 kpc.

Irregular galaxies are modelled as one zone objects and are assumed to assemble all their gas by means of a continuous infall of primordial gas and to form stars at a lower rate than the other morphological types. Their stellar populations appear to be mostly young, their metallicity is low and their gas content is large. All these features indicate that these galaxies are poorly evolved objects. Furthermore, irregular galaxies are allowed to develop moderate galactic winds which do not halt the star formation as in the spheroids (Bradamante et al. 1998).

2.1 The chemical evolution models

The equation that describes the evolution of the i-th element has the following form:

$$\frac{dG_i(t)}{dt} = -\psi(t)X_i(t)$$
$$+ \int_{M_L}^{M_{Bm}} \psi(t-\tau_m)Q_{mi}(t-\tau_m)\phi(m)\,dm$$
$$+ A\int_{M_{Bm}}^{M_{BM}} \phi(m)$$
$$\cdot \left[\int_{\mu_{min}}^{0.5} f(\mu)\psi(t-\tau_{m2})Q_{mi}(t-\tau_{m2})\phi(m)\,d\mu \right] dm$$
$$+ (1-A)\int_{M_{Bm}}^{M_{BM}} \psi(t-\tau_m)Q_{mi}(t-\tau_m)\phi(m)\,dm$$
$$+ \int_{M_{BM}}^{M_U} \psi(t-\tau_m)Q_{mi}(t-\tau_m)\phi(m)\,dm$$
$$+ X_{Ai}A(t) - X_iW(t)\,. \qquad (1)$$

Where $G_i(t)$ is the normalized fractional mass of gas within a galaxy in the form of the element i:

$$G_i(t) = \frac{M_g(t)\,X_i(t)}{M_{tot}}\,, \qquad (2)$$

where M_{tot} and $M_g(t)$ are the total galaxy mass and the mass of gas at time t, respectively.

$$X_i(t) = \frac{G_i(t)}{G(t)} \qquad (3)$$

represents the abundance in mass of the element i, the summation over all elements in the gas mixture being equal to unity. Thus, the quantity:

$$G(t) = \frac{M_g(t)}{M_{tot}}, \qquad (4)$$

is the total fractional mass of gas present in the galaxy at time t. In the case of spiral disks $M_g(t)$ and M_{tot} are replaced by the corresponding surface densities $\sigma(r,t)$ and $\sigma(r,t_G)$

The first term on the right hand side of eq. 1, including the star formation rate $\psi(t)$, represents the rate at which each element disappears from the ISM owing to the star formation.

The second term is the rate at which each element is restored into the ISM by single stars with masses in the range $[M_L,\ M_{Bm}]$, where M_L is the minimum stellar mass contributing, at a given time t, to chemical enrichment ($\simeq 0.8M_\odot$) and M_{Bm} is the minimum total binary mass of systems which can give rise to Type Ia SNe (3 $M_\odot$, Matteucci & Greggio 1986). The quantity $Q_{mi}(t-\tau_m)$ indicates the fraction of mass restored by the stars in form of an element i that can be produced or destroyed in stars or both. This is the so-called *"production matrix"* (Talbot & Arnett 1973).

The third term represents the enrichment due to binaries which become Type Ia SNe, i.e. all the binary systems with total mass in the range between M_{Bm} and M_{BM}, with M_{BM} being the maximum total mass of a binary system which can give rise to Type Ia SNe and is equal to 16 $M_\odot$ (8 + 8 $M_\odot$). The model adopted for the progenitors of the Type Ia SNe is the single degenerate one as in

Matteucci & Greggio (1986). The parameter A represents the fraction of binary stars giving rise to Type Ia SNe, and although its real value is unknown it is fixed in order to reproduce the observed present time SN Ia rate. This parameter obviously depends on the adopted IMF and, in general, values between 0.05 and 0.09 are adopted. This ensures to reproduce the actual SN Ia rate both in the Milky Way and in other galaxies. It is worth noting that, in this term, the quantities ψ and Q_{mi} refer to the time $(t-\tau_{m2})$, where τ_{m2} indicates the lifetime of the secondary star of the binary system, which regulates the explosion timescale of the system. The coefficient $\mu = M_2/M_B$, is the ratio between the mass of the secondary component and the total mass of the binary system, while $f(\mu)$ is the distribution function of this ratio. It is calculated on a statistical basis indicating that values close to 0.5 are preferred. Its analytical expression can be written as:

$$f(\mu) = 2^{(1+\gamma)}(1+\gamma)\mu^\gamma, \qquad (5)$$

with $\gamma = 2$ as a parameter (Greggio & Renzini 1983) and $\mu_{\min}$ is the minimum mass fraction contributing to the SNIa rate at the time t, and is given by:

$$\mu_{min} = max\left[\frac{M_2(t)}{M_B}, \frac{M_2 - 0.5M_B}{M_B}\right]. \qquad (6)$$

The fourth term of eq. 1 represents the enrichment due to stars in the range $[M_{Bm}, M_{BM}]$ which are single or, if binaries, do not produce a SNIa event. All the stars in this range with mass larger than $8M_\odot$ are assumed to explode as core collapse supernovae.

The fifth term represents the contribution to the chemical enrichment coming from stars more massive than M_{BM} (supposed to explode like Type II and $I_{b/c}$ SNe). In all the models the upper mass limit contributing to chemical enrichment is assumed to be 100 $M_\odot$.

Finally, the last two terms are the rate of accretion of matter with primordial abundances X_A, and the outflow rate for the element i, respectively.

2.1.1 The Star Formation Rate

The main feature characterizing a particular morphological galactic type is represented by the prescription adopted for its star formation history. In the case of elliptical galaxies the SFR ψ has the simple form given by:

$$\psi = \nu G(t), \qquad (7)$$

where ν is the star formation efficiency, namely the inverse of the typical time scale for star formation, and assumed to be 15 Gyr^{-1}.

In the case of irregular galaxies, a continuous star formation rate is assumed as in eq. 7, but characterized by a lower efficiency than the one adopted for ellipticals (0.1 Gyr^{-1} in this case).

In the case of spiral galaxies the formulation is the following (see Matteucci & Francois 1989 and Chiappini et al. 1997):

$$\psi(r,t) = \nu \cdot \left[\frac{\sigma(r,t)}{\sigma(r_\odot,t)}\right]^{2(k-1)} \cdot \left[\frac{\sigma(r,t_G)}{\sigma(r,t)}\right]^{(k-1)} \cdot G^k(r,t), \qquad (8)$$

Morphological Type	M_{tot} $(M_\odot)$	τ_{inf} (Gyr)	ν (Gyr^{-1})	R_{eff} (Kpc)
Ellipticals	10^{11}	0.3	15	3.0
Spirals	4×10^{10}	7.0	1.0	3.5
Irregulars	10^{10}	0.5	0.1	1.0

Table 1. Model parameters for the galaxies reproduced in this work. M_{tot} is the baryonic mass, R_{eff} is the effective radius, τ_{inf} is the infall timescale and ν is the star formation efficiency. For spirals we indicate the average infall time scale for the disk.

where ν is set in this case equal to 1 Gyr^{-1}, $\sigma(r,t)$ is the total surface mass density at a given radius and at a given time, $\sigma(r_\odot,t)$ is the total surface mass density at the position of the Sun (set equal to 8.0 Kpc). Finally $\sigma(r,t_G)$ is the surface mass density at present time. The exponent k is assumed equal to 1.4, as suggested by Kennicutt (1998).

All these models are tuned to reproduce at best the main observed properties of local galaxies of different morphological type. In Table 1 we show the main characteristics of the galaxies of different morphological type that we use in this work. It is important to stress that in our models, we consider only one galaxy per morphological type and take it as representative of the whole population. For the spiral galaxy we take the average SF and metallicity of the disk.

In Figure 1 we show the histories of star formation of the galaxies of different morphological type described above, for a Salpeter (1955) IMF. It is worth noting that for a spiral like the Milky Way an IMF steeper than the one used is usually adopted. Here we assume Salpeter (1955) IMF for all galaxies because the CSFR derived observationally is obtained by means of this IMF. As it is clear from the Figure a typical elliptical (10^{11} $M_\odot$ of luminous mass) experiences a high burst of star formation lasting for about 0.6 Gyr with a maximum peak of more than ~ 100 $M_\odot yr^{-1}$. After such a period, the star formation ceases abruptly owing to the onset of the galactic wind. The spiral disk is characterized by a continuous SFR with a large peak around $1\sim 2$ Gyr of less than ~ 10 $M_\odot yr^{-1}$ and a present time value of ~ 2 $M_\odot yr^{-1}$ (for the Milky Way). Finally, the irregular galaxy forms stars at a rate smaller than the previous morphological types, with an increasing SFR that reaches a maximum of less then 1 $M_\odot yr^{-1}$, with a smaller present value, due to the onset of the galactic wind.

2.2 The photometric model

To study the evolution of the photometric properties of galaxies, we use the spectro-photometric code GRASIL (Silva et al. 1998). Its starting point is the output of a chemical evolution code that follows the time evolution of SFR, metallicity (Z) and gas fraction. The building blocks of galaxy photometric models are the library of isochrones and the stellar atmospheric models. GRASIL is based on the Padova stellar models (Bertelli et al. 1994), with a major difference consisting in the computation of the effects of dusty envelops around AGB stars, and on the stellar atmospheric models by Kurucz (1992). The single stellar populations (SSPs) span a range from 1 Myr to 18 Gyr for what concerns ages, and $Z = 0.004, 0.008, 0.02, 0.05, 0.1$ for the metallicities (keeping the relative proportion of the metals
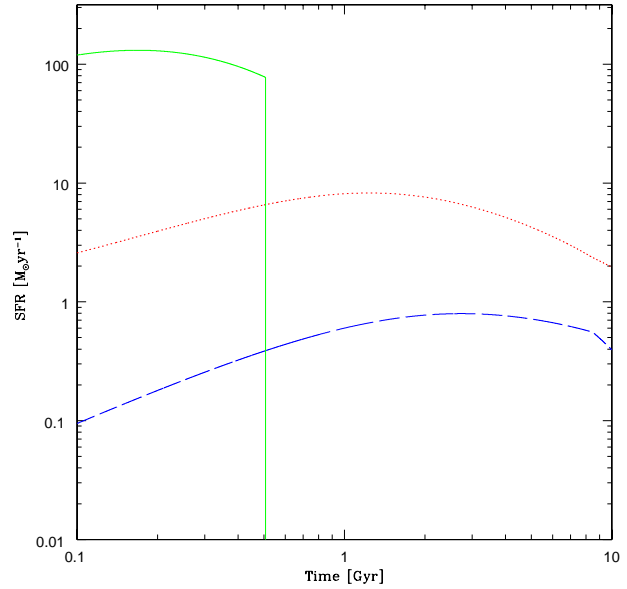
Figure 1. Star formation rates as a function of time, for a typical elliptical of 10^{11} $M_\odot$ (green solid line), spiral of $\sim 4\times 10^{10}$ $M_\odot$ (red dotted line) and irregular of 10^{10} $M_\odot$ (blue dashed line) galaxy.

equal to the solar partition). At this point, the spectral synthesis is performed summing up the spectra of each stellar generation provided by the SSP of the appropriate age and metallicity, weighted by the SFR (ψ) at the time of the star birth. The flux at a given wavelength is defined as:

$$F_\lambda(t_G) = \int_0^{t_G} \psi(t)\times SSP_\lambda(t_G - t, Z(t))\, dt, \qquad (9)$$

where $F_\lambda(t_G)$ is the integrated monochromatic flux at the present time t_G and $SSP_\lambda(t_G - t, Z(t))$ is the integrated monochromatic flux of an SSP at age t and metallicity Z. If the effects of dust are neglected (as in our case) the spectral energy distribution (SED) is simply given summing up the spectra of all stars.

2.3 The luminosity evolution of galaxies

To derive the CSFR, it is of fundamental importance the knowledge of the relative distribution of galaxies, of any morphological type, as a function of redshift. This can be done through the LF, which gives the distribution of galaxies per unit volume in the luminosity interval $[L,\ L + dL]$. The LF is well reproduced by the Schechter (1976) function:

$$\Phi(L)\frac{dL}{L^*} = \phi^*\left(\frac{L}{L^*}\right)^{-\alpha} e^{(-L/L^*)}\frac{dL}{L^*}, \qquad (10)$$

where ϕ^* is the number of galaxies per unit volume; L^* is the characteristic luminosity which separates bright sources from faint sources and α is the slope of the luminosity function. Different determinations of the local LF exist (see de Lapparent 2003 for a review) and they show several differences, in the sense that the parameters of the Schechter

Morphological Type	M^*	α	ϕ^*
Ellipticals	−19.37	−1.00	4.4
Spirals	−19.43	−1.11	8.0
Irregulars	−19.78	−1.81	0.2

Table 2. Parameters of the LF as defined in Marzke et al. (1998). Here M^* refers to the magnitude of the galaxy at the break, ϕ^* refers to the normalization of the LF (expressed in Mpc^{-3}) and α is the slope of the LF.

function are not fully constrained by observations. The luminosity function can be measured in several bands, obviously depending on the redshift regime under investigation. In this work, we make use of the determination of the local B-band luminosity function of Marzke et al. (1998), that has the characteristic of considering separately the different galactic morphological types. For each morphological type the parameters of the LF are summarized in table 2.

Once we have the LF, we can compute the *luminosity density (LD)*, which is what is really observed. The luminosity density, in a given band, is defined as the integrated light radiated per unit volume from the entire galaxy population. It stems from the integral over all luminosities of the observed luminosity function:

$$\rho_L = \int \Phi(L) \left(\frac{L}{L^*} \right) dL. \qquad (11)$$

At $z = 0$, the LDs for the single galaxy types are given by the above integral of the present time luminosity functions of Marzke et al. (1998). At redshifts other than zero, for each morphological type we consider the luminosity evolution obtained with the spectrophotometric code.

3 RESULTS

As already pointed out, the CSFR is not a directly measurable quantity. It can be inferred only from the measurement of the luminosity density in different wavebands and then converted into SF by means of suitable calibrations. Its first determination was made by Lilly et al. (1996) (at 2800 Å, 4400 Å, and 1 μm), followed in the subsequent years by Hogg et al. (1998) (using the [OII] line) and Wilson et al. (2002) (in the UV). These studies constrained the CSFR from $z = 0$ to $z = 1$, establishing that it is steadily increasing in that range. The CSFR seems to peak around $z \sim 2-3$ and then decrease at higher redshifts, where there is not a well defined trend. For example Bouwens et al. (2008) on the basis of optical and UV data and Hopkins (2004) on the basis of a compilation of data taken in different bands, found that the CSFR from roughly $z \sim 3$ to $z \sim 9$ is steadily decreasing. On the other hand, Kistler et al. (2009), on the basis of the gamma ray burst (GRB) data from *Swift* found a CSFR that is roughly constant from $z \sim 4$ to $z \sim 8$.

3.1 The cosmic star formation rate

By means of the star formation histories of galaxies of different morphological type and their photometric evolution we

can calculate the CSFR according to the method adopted by Calura & Matteucci (2003):

$$\dot{\rho}_*(z) = \sum_i \rho_{Bi}(z) \left(\frac{M}{L} \right)_{Bi} (z) \psi_i(z), \qquad (12)$$

where $\dot{\rho}_*(z)$ is the SFR density, ρ_{Bi} is the B-Band luminosity density, $\left(\frac{M}{L} \right)_{Bi}$ is the B-band mass-to-light ratio and ψ_i (expressed in yr^{-1}) is the star formation rate per unit mass of the i-th morphological type.

In this work, we make use of the B-band luminosity, because it is a good star formation tracer since hot massive stars emit in this band.

In principle, the CSFR, could be computed simply by summing the SFR of each galaxy type multiplied by the corresponding number density. However, this simple approach would not allow us to explore in detail the case in which the slope of the LF varies with redshift (see section 3.1.3). We tested that the two approaches lead to the same result.

3.1.1 The Pure Luminosity Evolution Scenario

Here we describe the determination of the CSFR in the framework of a PLE scenario. With pure luminosity evolution, we mean that galaxies of all morphological types are supposed to form at high redshift and then to evolve only in luminosity and not in number. We also assume that the slope of the LF is constant with redshift. In this context, galaxies are assumed to be isolated, i.e. the effects of mergers or interactions are irrelevant at all redshifts, and it is assumed that they start forming stars all at the same time.

In this simple approach, the differences between the various morphological types should be ascribed only to their different star formation histories. Early-type galaxies (i.e. ellipticals, bulges and S0) are dominated by old stellar populations so they must have formed their stars with high efficiency and in a short period, while late-type galaxies (i.e. spirals and irregulars) should have formed stars for the whole Hubble time, as seen in Fig. 1.

In Figure 2 we can see the predicted evolution of the luminosity density for ellipticals, spirals and irregulars, in the U (centered at 3650 Å), B (centered at 4450 Å), I (centered at 8060 Å) and K (centered at 21900 Å) band. These evolutions are computed by adopting the SFRs of Fig. 1 and constant slope and number density in the luminosity function.

From the Figure it is clear that, at early times in every band, the luminosity density is dominated by the light emitted by elliptical galaxies. This is obviously due to the fact that in the monolithic scenario they all suffer a strong initial burst of star formation which lasts for < 1 Gyr and then evolve passively. At this time a galactic wind develops and star formation stops, so their luminosity in the U and B bands, where young, newborn stars emit, begins rapidly to decrease. On the other hand, spirals form stars continuously and the decrease in luminosity in the U and B band should be ascribed mostly to the consumption of their gas reservoir. Finally, also irregulars form stars for the entire cosmic time but their luminosity density is lower than that of the other morphological types due to their low star formation. Their
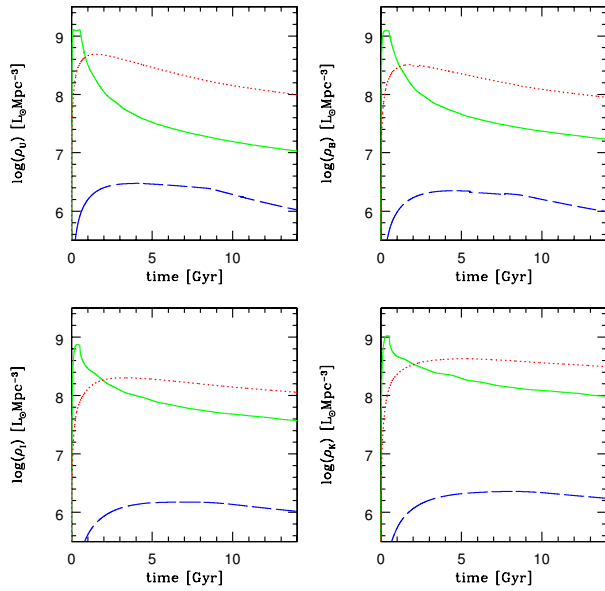
Figure 2. Prediction of the luminosity density evolution for galaxies of different types in U (top left), B (top right), I (bottom left) and K (bottom right) band respectively, in the case of pure luminosity evolution. Here the x-axis represents the elapsed time since z=10. Solid green line refers to ellipticals, red dotted line to spirals and long dashed blue line to irregulars.

luminosity density is also decreased by the onset of galactic winds at late times.

The I and K bands are dominated by the light emitted by less massive, long living stars. Also in this case, ellipticals are the main sources at early times, while spirals become dominant for cosmic time $> 2 \; Gyr$. However, the difference in the values reached by ellipticals and spirals is less pronounced than in U and B bands. The luminosity density of spirals, after an initial phase of constant increase lasting $\sim 3 \; Gyr$ is observed to decrease slowly in the I band and to be quite constant in the K band. Irregulars, also in this case have values lower than ellipticals and spirals which tend to decrease very slowly through the whole cosmic time.

The PLE model belongs to the category of the so-called *"backward evolution"* models (Tinsley & Danly 1976); these models start from a well known and well constrained description of the local Universe to reconstruct the evolution of galaxies back to their formation.

In our model, all the galaxies are supposed to form at $z = 10$. This choice is motivated by the fact that more and more objects are revealed at $z > 5$ (Mobasher et al. 2005,Vanzella et al. 2008), with evidences of a $z \sim 10$ detection (Bouwens et al. 2011b). The predicted CSFR is shown in Figure 3; for comparison we plot in the same Figure also the CSFR as obtained by Calura & Matteucci (2003) who adopted very similar assumptions and star formation histories.

As it can be seen, both models show some discrepancies when compared with the observational data. In our case, the discrepancy begins at $z \sim 0.5$ and it is particularly evident in the redshift interval running from ~ 0.5 to ~ 5. Here
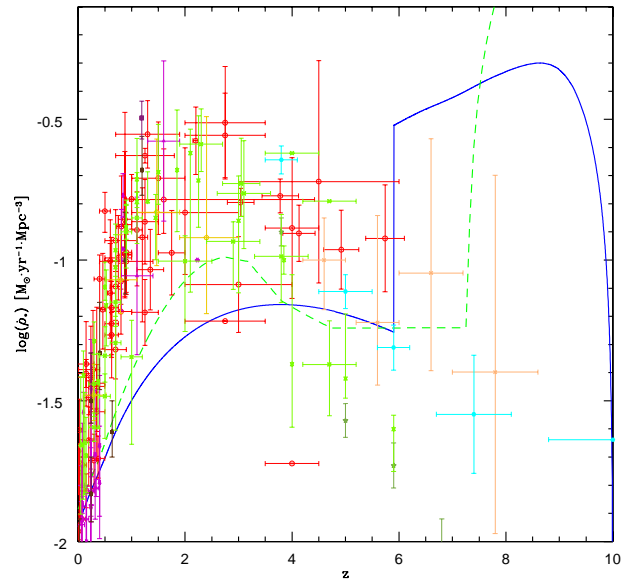
Figure 3. Cosmic star formation history in the case of pure luminosity evolution. Blue solid line, model described in this work; green dashed line model from Calura & Matteucci (2003). Points are taken from: Hopkins (2004) red open circles, Ly et al. (2007) brown squares, Takahashi et al. (2007) purple open squares, Li (2008) cyan open hexagons, Seymour et al. (2008) yellow pentagons, Kistler et al. (2009) orange crosses, Ly et al. (2011) magenta triangles, Bouwens et al. (2011a) green open stars, Cucciati et al. (2011) light green crosses.

we underpredict the observed values by a factor of ~ 3. This is the redshift interval in which only spirals and irregulars contribute to the cosmic star formation history. Also the Calura & Matteucci CSFR suffers of the same problem when compared with data. On the other side, at high redshift, our model seems to overpredict the data, as well as that of Calura & Matteucci. The high observed peak is to ascribe to ellipticals which, in order to reproduce the local observational features, (like the increase of the $[Mg/Fe]$ ratio with galactic mass) have to form stars in a short time interval (lasting less than 1 Gyr, Matteucci 1994). This implies that the SFR of these objects must lie in the range $\sim 100 - 1000 \; M_\odot yr^{-1}$. At $z \sim 6$ ellipticals stop to form stars and the CSFR decreases abruptly. The discrepancies with the model of Calura & Matteucci (2003) can be explained through the differences in the parameters adopted in the chemical evolution models and in the different photometric code used. In fact, in Calura & Matteucci (2003), the photometric code of Jimenez et al. (1998) was adopted. Moreover, the chemical model for the ellipticals adopted by Calura & Matteucci (2003) is a closed box one, whereas our model includes gas infall.

3.1.2   The Number Density Evolution Scenario (NDE)

In this section, we describe a different approach for the calculation of the CSFR. In what follows we introduce a scenario in which we let the number density of galaxies to evolve with redshift while the SFHs of galaxies are the same of Fig. 1.

The main consequence of relaxing the hypothesis of the constancy of the number density of galaxies is that we consider galaxy interactions. It has been claimed that giant ellipticals could form, as the result of the occurrence of 1 to 3 major dry-mergers during galactic lifetime (Pipino & Matteucci 2008 and reference therein) and this view is in agreement with the observations. Moreover it has been observed that the fraction of dry-mergers increases with redshift from $z \sim 1.2$ to $z = 0$ (Lin et al. 2008).

To include the number density variation we modify the expression of the luminosity function as defined in eq. 10, letting the parameter ϕ^* (i.e. the number density of galaxies) to vary with the redshift. The new formulation of the luminosity function is:

$$\Phi(L)\frac{dL}{L^*} = \phi_0 \cdot (1+z)^\beta \left(\frac{L}{L^*}\right)^{-\alpha} e^{(-L/L^*)}\frac{dL}{L^*}, \qquad (13)$$

where $\phi_0 = \phi^*(z=0)$, i.e. the present time number density of galaxies. This model is constrained in order to reproduce the number densities observed at $z = 0$ by Marzke et al. (1998).

We let the parameter β to run from -6 to $+6$ in steps of 0.2. The choice of this interval has been made in order to explore a set of values as wide as possible without giving us meaningless results and, at the same time, letting us to test cases of extreme number density variation. For each value of β, we calculate the luminosity density using the modified version of the Schechter function. Then, using the star formation histories depicted in section 2.1.1, we determine the star formation rate density, using the equation 12.

We perform a careful check of the contribution to the total CSFR from the different morphological types, and on its basis we decide to let only spirals and ellipticals to evolve. Therefore, we consider the number density of irregulars constant through the cosmic time. The reason resides in their contribution to the total CSFR, that is, at any redshift, two orders of magnitude lower than the one of ellipticals and spirals and therefore negligible. Our best values of the β parameter for each morphological type are:

- Ellipticals: $\beta = -0.8$;
- spirals: $\beta = 1$;
- irregulars: $\beta = 0$.

This means that the number density of ellipticals is supposed to increase from $z = 10$ to $z = 0$ (with $\sim 15\%$ of ellipticals already in place at $z = 10$). The opposite behaviour is predicted for spirals, which are supposed to decrease with decreasing redshift. Under these assumptions, there is a possible interpretation in terms of galaxy formation. For example, the predicted number density evolution could mean that a large fraction of elliptical galaxies can form thanks to dry mergers of spirals, as proposed by Toomre & Toomre (1972) and Naab & Burkert (2003). Since we are considering only dry-mergers it means that the merging process quenches the star formation in the progenitors and that the residual gas is lost. From our model we can see that the number density of spirals decreases of roughly 60% from $z \sim 2$ to $z \sim 0$, and of 50% from $z \sim 1$ to $z = 0$. This is in good agreement with Boissier et al. (2010) who found a decrease of 50% of Milky Way siblings from $z \sim 1$ to $z = 0$, indicating this percentage as a lower limit. In Figure 4 we show our best

model for the CSFR in the case of number density evolution. From the plot we can see that the peak observed in the PLE scenario completely disappears. The model seems to better reproduce the high redshift trend if the error bars are taken into account. Also in the redshift interval between 0 and ~ 5 the agreement is improved although the curve is still slightly lower than the data, but this is a problem common to all the other models of CSFR, as we will see later. Also in this case we underpredict the decrease of the CSFR between $z \sim 2$ and $z = 0$. This, in principle, can be due to the lack in our models of strong starburst galaxies at low and intermediate redshift (see e.g. Elbaz et al. 2011), even if as claimed by Rodighiero et al. (2011) starbursts seem to account only for the 10% of the SFR density at $z \sim 2$. On the other hand, our predicted slope of the CSFR in this redshift range good as well as for the model of van de Voort et al. (2011). These authors using cosmological smoothed particle hydrodynamics simulations, explain this drop with a decline in the cold-accretion rate density on to haloes and with AGN feedback that decreases the contribution to the CSFR of the gas accreted in the hot mode.

In Figure 5 we show the predicted evolution of the luminosity density, for our best model, in the case of number density evolution. Comparing these predictions with the ones in Figure 2, it is possible to see that in this case spirals dominate the luminosity density in every band and at any epoch, at variance with the PLE case.

It must be said that the variation of the number density of galaxies of different morphological types is still matter of debate, since there is, in general, no concordance among various authors. For example, Totani & Yoshii (1998) found that, parametrizing the comoving number density of $E/S0$ as proportional to $(1+z)^\gamma$, the favoured value for γ is -0.8 ± 1.7, in perfect agreement with our value. This analysis is valid in the redshift range $0.3 < z < 0.8$, and the large error is due to the limited redshift range of their sample. de Lapparent et al. (2004), using data from the ESS (ESO-Sculptor Survey), found a number density evolution of late-type galaxies following the same parametrization, with $\gamma = 2 \pm 1$. On the other hand, for example Lilly et al. (1998) found at $z < 1$ an evolution of large disk structures (with a bulge-over-total ratio $B/T > 0.5$) following a $(1 + z)^\gamma$ relation, with $\gamma = \pm 0.5$, lower than the one found in our model.

Even more challenging is to asses the evolution at high redshift, since very deep surveys are required and the correspondence between actual galaxies and their high z counterparts is not firmly established. This causes a loss of information about the morphology of the various objects giving controversial results. Moreover, the uncertain dust corrections and the adopted IMF (Salpeter 1955) used to derive the CSFR, could underestimate the actual CSFR. Therefore, we do not completely exclude that the CSFR could be constant or increasing at high z.

3.1.3 The Variation of α

In this section we describe a modification of the Schechter function in which we consider the evolution with redshift of the slope of the LF for galaxies of different morphological type. We start again from the LF as defined in sec. 2.3, and assume that $\alpha = \alpha_0(1+z)^\beta$, where $\alpha_0 = \alpha(z=0)$ is the
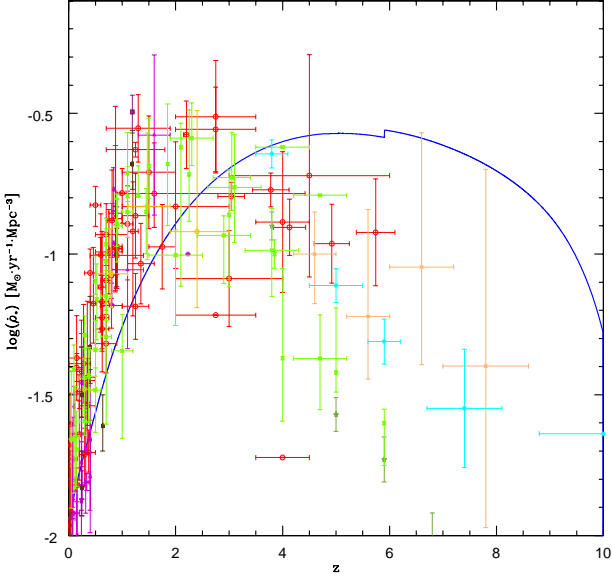
Figure 4. The cosmic star formation history in the number density evolution scenario. Blue line refers to model results. Data points are the same described in Figure 3.
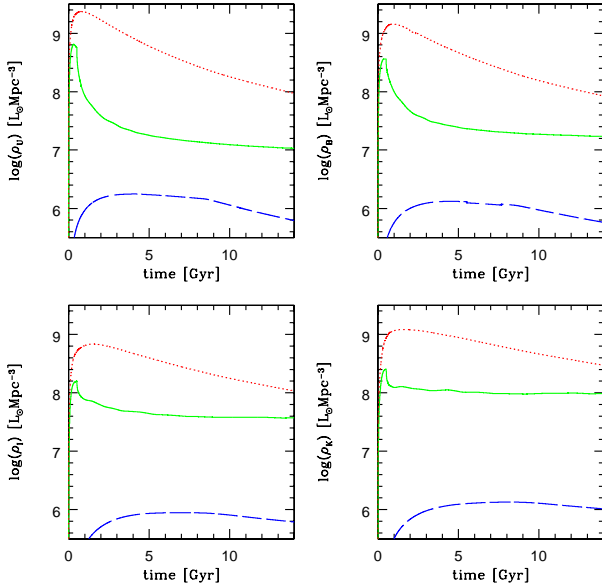
Figure 5. Prediction of the luminosity density evolution for galaxies of different types in U (top left), B (top right), I (bottom left) and K (bottom right) band respectively in the case of number density evolution (best model). Here the x-axis represents the elapsed time since z=10. Solid green line refers to ellipticals, red dotted line to spirals and long dashed blue line to irregulars.
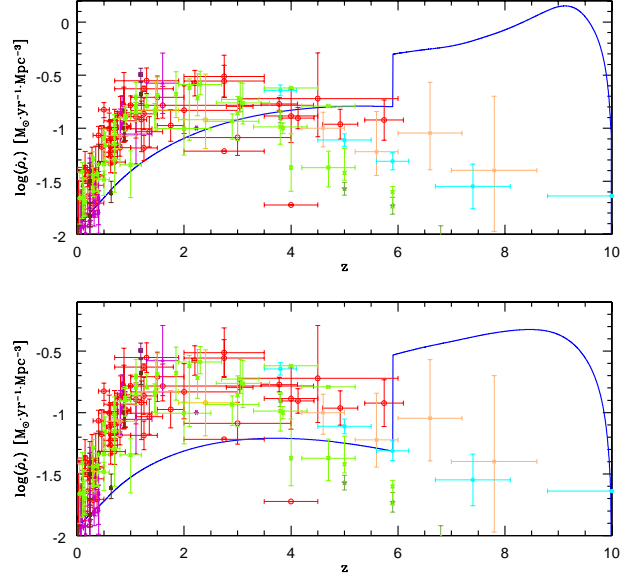
Figure 6. The CSFH in the case of variation of the LF slope α. Here we show the cases corresponding to $\beta = 0.4$ (top panel) and $\beta = -0.2$ (bottom panel). Blue lines indicate the results of the model. Data points are the same described in Figure 3. Note the different y-axis scale adopted for clarity.

slope of the LF at present time and β is a free parameter. Therefore, the LF assumes the form:

$$\Phi(L)\frac{dL}{L^*} = \phi^* \cdot \left(\frac{L}{L^*}\right)^{[-\alpha_0(1+z)^\beta]} e^{(-L/L^*)}\frac{dL}{L^*}. \qquad (14)$$

This means that at any redshift we change the slope of the LF. As in the case of the number density evolution, we let β to run from -6 to $+6$ in steps of 0.2, and in no case we have found an improvement in fitting the data relative to the pure luminosity or number density variation scenarios. From the observational point of view, there are some suggestions of variations of the slope of the LF but referred to the whole population of galaxies, without differentiating for morphological types. For example, Reddy & Steidel (2009) found that $\alpha = -1.1$ locally and increases up to ~ -1.7 at high redshift (from z=3 to 6). From our numerical experiments this case corresponds to $\beta \sim 0.3$. We can exclude all the cases with $\beta > 0.4$ and those with $\beta < -0.2$ since they predict values of α which are very much outside the observed range, and also a CSFR very much at variance with observations.

In Figure 6 we show the case $\beta = 0.4$ (top panel) which is similar to the suggested observational variation (Reddy & Steidel 2009), and the case $\beta = -0.2$ (lower panel). Therefore, although we do not exclude a variation of the slope of the LFs of galaxies, we can conclude that the cases of α variations are providing a fit to the CSFR which is worse than the case in which there is number density variation, as shown in Figure 4. Finally, we run several models by varying both ϕ^* and α and we did not find any combination of parameters which can fit the observed CSFR better than our best case with ϕ^* only variation. In Figure 7 we show
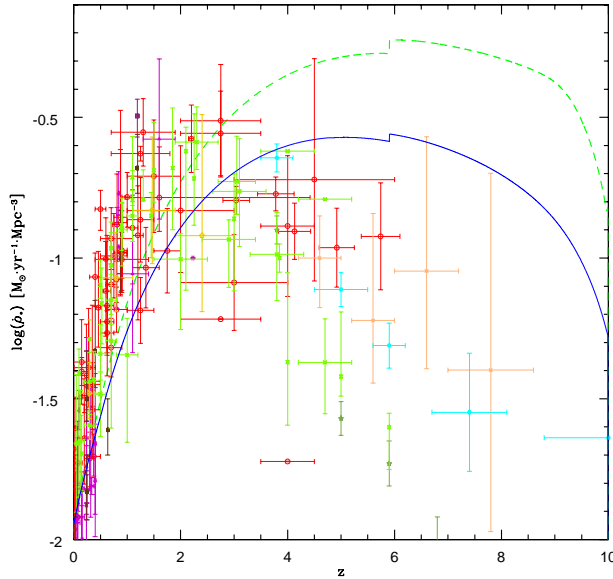
Figure 7. Comparison between our best model with NDE (blue solid line) and a model with both NDE (the same as the best model) and α evolution (green dashed line). Data points are the same described in Figure 3.

a comparison between a model with the same variation of ϕ^* as our best model (see section 3.1.2) and a model with the same ϕ^* variation plus a variation of α, obtained with $\beta = 0.3$ for ellipticals and $\beta = 0.2$ for spirals and irregulars. As one can see, the agreement between the model with variable α and ϕ^* does not fit the data as well as our best model.

3.1.4 Comparison with other determinations

In Figure 8 we show the results of several determinations of the CSFR that we compare to our model predictions, in particular with the PLE and with our best model with NDE. The determinations of the CSFR we use for this comparison are:
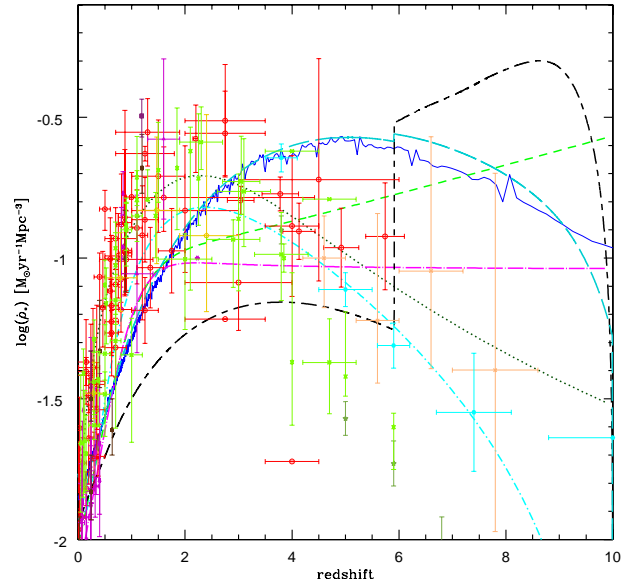
- *Steidel et al. (1999):*
  It is based on a sample of star-forming galaxies at $z \gtrsim 4$. The corresponding CSFR based on their data has been then parametrized by Porciani & Madau (2001) (their model SF2).
- *Cole et al. (2001):*
  Combining the data of the Two Micron All Sky Survey (2MASS) Extended Source Catalog and the 2dF Galaxy Redshift Survey, they produce an infrared selected galaxy catalogue. They use it to estimate the galaxy LF and to infer the total mass fraction in stars. Then they use their results together with the data of Steidel et al. (1999) to obtain a parametric fit of the CSFR. Their parametric form has also been used by Hopkins & Beacom (2006).
- *Porciani & Madau (2001):*
  Here we refer to their model SF3. It is a parameterization of the CSFR based on the data collected by the Burst and Transient Source Experiment (BATSE). It is adopted to test

Figure 8. A compilation of determinations of the CSFH, compared to the results of this work. Models are from: Steidel et al. (1999) magenta long dash-dotted line, Porciani & Madau (2001) green short-dashed line, Cole et al. (2001) dark green dotted line, Menci et al. (2004) blue solid line, Strolger et al. (2004) cyan dot short-dashed line, this work (PLE) black short-dashed long-dashed line, this work (NDE) turquoise long dashed line. Data point are the same as Figure 3.

the hypothesis that the rate of GRBs traces the global star formation history of the Universe.
- *Strolger et al. (2004):*
  It is a model based on a modified version of the parametric form suggested by Madau et al. (1998), taking into account dust extinction. Model parameters are determined fitting the collection of measurements of the CSFR of Giavalisco et al. (2004).
- *Menci et al. (2004):*
  Prediction from a semi-analytic model for galaxy formation in the framework of the hierarchical clustering scenario.

For further information we address the reader to the above mentioned papers.

From Figure 8 it is possible to see that our model with number density evolution shows a complete agreement with the semi analytical model of Menci et al. (2004) and, in general, shows a better agreement with the data, if compared to the determinations of Steidel et al. (1999) and Porciani & Madau (2001). For what concerns the PLE model, this presents lower values than the other CSFRs, in the redshift range $[0 - 6]$. On the other hand, for $z > 6$ it exceeds all the other predictions considered here, as we have discussed already.

3.1.5 The cosmic ISM mean metallicity

Here we compute the evolution of the cosmic, luminosity weighted, mean interstellar metallicity of the galaxies of different morphological type. With this definition, we indicate the mean metallicity of the gas from which stars are
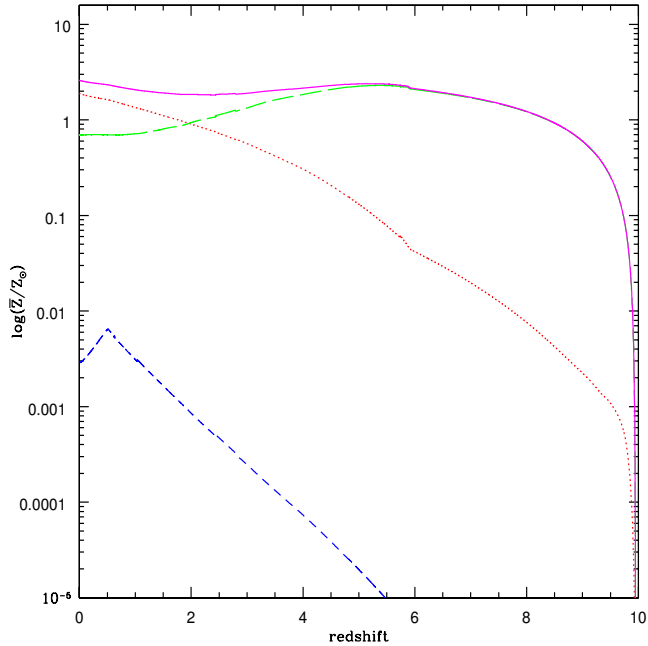
Figure 9. The cosmic luminosity weighted mean metallicity relative to the Sun in the case of pure luminosity evolution. Magenta solid line: total; red dotted line: spirals; green long-dashed line: ellipticals; blue dashed line: irregulars. All the values are normalized to the solar metallicty $Z_\odot = 0.0134$, from Asplund et al. (2009).

Figure 10. The cosmic luminosity weighted mean metallicity relative to the Sun in the case of number density evolution. Magenta solid line: total; red dotted line: spirals; green long dashed line: ellipticals; blue dashed line: irregulars. All the values are normalized to the solar metallicty $Z_\odot = 0.0134$, from Asplund et al. (2009).
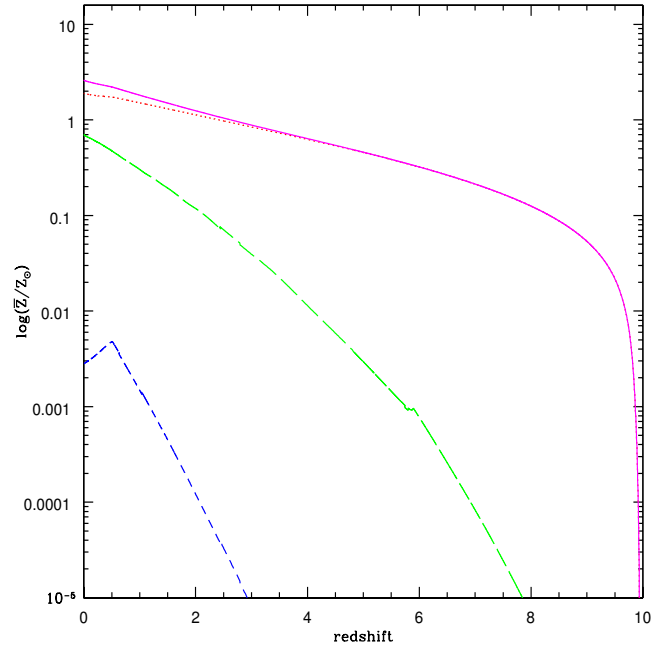
born, in a unitary volume of the Universe. As suggested by Kulkarni & Fall (2002), we compute it through the following expression:

$$\bar{Z} = \frac{\int Z_i(L_i) L_i \Phi_i(L_i) \, dL_i}{\sum_i \int L_i \Phi_i(L_i) \, dL_i}, \tag{15}$$

where $Z_i(L)$ is the average interstellar metallicity in a galaxy of luminosity L_i, at any given cosmic time, and of the i-th morphological type and $\Phi_i(L_i)$ is the luminosity function of the i-th morphological type.

We compute this quantity both in the case of PLE and NDE, using the metallicity evolutions obtained with the chemical evolution models, together with the local B-band luminosities obtained with the spectrophotometric code. The parameters of the local luminosity functions, are from Marzke et al. (1998), as in the previous paragraphs.

From Figure 9 it is clear that in the PLE scenario ellipticals dominate the mean galactic metallicity throughout the whole cosmic time. This is due to their higher average metallicity compared to spirals and irregulars and to the constant number density of all galaxies. The spiral galaxies are the second most important contributors to the cosmic chemical enrichment, whereas irregulars give a negligible contribution. We can see that our model is in agreement with Calura & Matteucci (2004) who found that for $z \gtrsim 6$ the main metal producers are ellipticals whereas for $z \lesssim 2$ the main sources of metals production are spirals. It is worth noting that, the decrease of the luminosity weighted metallicity of ellipticals is due to the fact that, at $z \sim 6$ in our model, ellipticals stop forming stars and from that moment on their B-band luminosity abruptly decreases. Also spirals decrease their B-band luminosity but mildly since their star

formation lasts for the whole cosmic time. We note that in this case two distinct effects are involved: the metallicity which is increasing and the luminosity which is decreasing with decreasing z.

In Figure 10 we show the same as in Figure 9 but under the hypothesis of number density evolution. In particular, we show the results of our best model, as described in section 3.1.2. The most evident fact in this case is that spirals, instead of ellipticals, are the main contributors to the total cosmic luminosity weighted mean metallicity. However, we need further investigation to better interpret this result. It has to be considered that this quantity cannot be compared directly with observations, since it is a cosmic average, while measurements are performed in single objects. Another important thing we note is that, in this case the cosmic luminosity weighted mean metallicity of ellipticals is increasing throughout the whole cosmic time. This can be explained by the fact that the decreasing of the B-band luminosity is compensated by the increase of their number density at lower redshift. We also find that our present time value of the cosmic luminosity weighted mean metallicity of the ISM in all galaxies and in each galaxy formation scenario is $\sim 2.4\,Z_\odot$, a value that is slightly higher than $1.3\,Z_\odot$ as found by Calura & Matteucci (2004). This is partly due to the fact that we adopt the solar metallicity of Asplund et al. (2009), that is lower than the $Z_\odot$ adopted in the previous paper.

This average metallicity is not the global average metallicity of the Universe since we did not consider the metallicity of the intracluster and intergalactic medium.

4 DISCUSSION AND CONCLUSIONS

In this paper we computed the CSFR by means of detailed chemical and spectro-photometric models of galaxies of different morphological type (ellipticals, spirals, irregulars).These models well reproduce the main properties of local galaxies and have been tested in the past on a variety of observational constraints (see Matteucci 2001). Models of galactic chemical evolution of galaxies contain a few free parameters such as the efficiency of star formation, the slope of the IMF in the case of external galaxies, the fraction of binary systems in the IMF giving rise to SNe Ia, the timescale for gas accretion and the efficiency of possible galactic winds. All these parameters should be fixed by reproducing the largest as possible number of observational constraints, so that the number of well fitted features outnumbers the number of free parameters. For the Milky Way we have many observational features to reproduce, such as the G-dwarf metallicity distribution, the solar abundances, the present time amount of gas, the present time SN rates, the star formation and gas infall rates, the abundance patterns in stars ([X/Fe] vs. [Fe/H], where X represents the abundance of a chemical elements). Then one should reproduce the abundance gradients of chemical abundances, star formation rate and gas distribution along the disk. For external galaxies, such as ellipticals, the number of constraints is less than for the Milky Way but still they are enough to counterbalance the number of free parameters involved in the models. The observational features to reproduce are: the Color-Magnitude diagram, the average metallicity (measured by Mg and Fe) of the stars, the abundance gradients in the stellar populations as a function of the galactocentric distance, the high $[\alpha/\text{Fe}]$ ratios measured in the dominant stellar population in the central part of these galaxies, the mass-metalicity relation and the $[\alpha/\text{Fe}]$ vs. mass relation, the Type Ia SN rate at the present time. This last features implies that the more massive galaxies show higher central $[\alpha/\text{Fe}]$ ratios than less massive ones. This is explained at the moment only by chemical evolution models of the knid presented here. Classical hierarchical models predict the contrary (see Thomas & al. 2002), while more recent semi-analytical models (e.g. De Lucia et al. 2006; Pipino et al. 2009) improve the situation but they still do not reproduce entirely this relation. In order to obtain an increase of the $[\alpha/\text{Fe}]$ ratio with galactic mass is enough to assume an increasing star formation efficiency with galactic mass. However, we cannot exclude a priori other solutions, such as a variable IMF from galaxy to galaxy, but this solution creates other problems (see Matteucci et al. 1998). Also the models for irregulars have been tested and they reproduce the metallicity, the amount of gas, the [C,N,O/Fe] vs. [Fe/H] relations, the SN rates for an average irregular galaxy. Therefore, we felt reasonably confident that the star formation histories suggested by these galaxy models could be used to compute the CSFR. We then adopted the histories of star formation predicted by such models and convolved them with the luminosity functions of galaxies. These LFs have been constrained to reproduce the observed local LFs. We first computed the CSFR under the assumption of pure luminosity evolution of galaxies, namely we did assume that the main parameters of the LF do not vary with redshift, in particular the number density of galaxies and the slope of the LF. By doing that,

we obtained results similar to those of Calura & Matteucci (2003). Then we computed the CSFR by assuming number density and slope evolution.

Our results can be summarized as follows:

• In the case of pure luminosity evolution of galaxies, the CSFR traces the star formation histories of galaxies. In the framework of our galaxy evolution models, ellipticals form at very high redshift in a very short interval of time and then evolve passively for the remaining galactic age. The spirals and even more the irregulars, instead, are forming stars continuously and at a much lower rate for the whole galactic lifetime. In this situation, we predict that the ellipticals are the dominant source of the cosmic star formation at very high redshift (from $z = 6$ to $z = 10$), whereas spirals start to dominate for $z < 6$. On the other hand the contribution of irregulars to both the CSFR and the cosmic chemical enrichment is found to be negligible. By comparing these model results with the available data for CSFR, we conclude that our models overpredict the CSFR at high redshift and underpredict it at low redshift. However, most of models for CSFR in the literature also underpredict this quantity at low redshift. For the high redshift situation we should take into account that the data for $z > 6$ are still very uncertain, especially because of the uncertain dust corrections and assumed IMF. Therefore, a conclusive statement on this point would be premature. For the low redshift we probably underestimate the amount of cosmic star formation, since we did not include massive starburst galaxies at intermediate and low redshift.

• In the case of number density evolution, by assuming that ellipticals were less at high redshift and their number increased at lower redshifts, and that the contrary happened to spirals, we obtain a CSFR in much better agreement with observations. This result could imply that many ellipticals formed by merging of spirals, as originally suggested by Toomre & Toomre (1972). In particular, our predicted number density evolution for ellipticals implies $\phi^* = \phi_0(1 + z)^{-0.8}$ in agreement with Totani & Yoshii (1998), whereas for spirals implies $\phi^* = \phi_0(1 + z)$ in agreement with de Lapparent et al. (2004) and Boissier et al. (2010). Possible criticism to the scenario of the dry mergers of spirals to form ellipticals is given by the fact that a dry merging process seems unrealistic in the light of the difficulty of reproducing the observed local chemical properties of ellipticals. In fact, it is well known that the chemical properties of spirals and ellipticals are different (e.g. different average metallicities and $[\alpha/\text{Fe}]$ ratios). By comparing our predicted CSFR with other determinations of the CSFR we found that it is similar to the CSFR of the hierarchical model of Menci & al. (2004).

• We tested also the case of a variation of the slope of the luminosity function with redshift and concluded that a variation of the slope similar to what is suggested by observations is not excluded, although it does not provide an improvement relative to pure luminosity evolution case and it predicts a CSFR in worse agreement with the data than the case of only galaxy number density variation. Also cases with both NDE and slope evolution at the same time do not provide better fits.

• We computed the cosmic, luminosity weighted, metallicity in the gas of galaxies and its evolution with redshift.

We found that, in the case of pure luminosity evolution, the ellipticals dominate the cosmic metal enrichment over the whole lifetime of the Universe. On the other hand, in the case of number density evolution, are the spirals to dominate the cosmic metal enrichment of the Universe. This is potentially an important result but it needs to be confirmed by future studies.

REFERENCES

Asplund M., Grevesse N., Sauval A.J., Scott P., 2009, ARAA 47, 481

Baugh C.M., Cole S., Frenk C.S., Lacey C.G., 1998, ApJ, 498, 504

Bertelli G., Bressan A., Chiosi C., Fagotto F., Nasi E., 1994, AAPS, 106, 275

Boissier S., Buat V., Ilbert O., 2010, AAP, 522, A18

Bouwens R.J., Illingworth G.D., Franx M., Ford H., 2008, ApJS, 686, 230

Bouwens R.J., Illingworth G.D., Labbé I., Oesch P.A., Trenti M., Carollo C.M., van Dokkum P.G., Franx M., Stiavelli M., González V., Magee D., Bradley L., 2011b, Nat, 469, 504

Bouwens R.J., Illingworth G.D., Oesch P.A., Labbé I., Trenti M., van Dokkum P., Franx M., Stiavelli M., Carollo C.M., Magee D., Gonzalez V., 2011a, ApJ, 737, 90

Bradamante F., Matteucci F., D'Ercole A., 1998, AAP, 337, 338

Calura F., Matteucci F., 2003, ApJ, 596, 734

Calura F., Matteucci F., 2004, MNRAS, 350, 351

Chiappini C., Matteucci F., & Gratton R., 1997, ApJ, 477, 765

Chiappini F., Matteucci F., Romano D., 2001, ApJ, 554, 1044

Cole, S., Lacey C.G., Baugh C.M., Frenk C.S., 2000, MNRAS 319, 168

Cole S., Norberg P., Baugh C.M., Frenk C.S., Bland-Hawthorn J., Bridges T., Cannon R., Colless M., Collins C., Couch W., Cross N., Dalton G., De Propris R., Driver S.P., Efstathiou G., Ellis R.S., Glazebrook K., Jackson C., Lahav O., Lewis I., Lumsden S., Maddox S., Madgwick D., Peacock J.A., Peterson B.A., Sutherland W., Taylor K., 2001, MNRAS, 326, 255

Cucciati O., Tresse L., Ilbert O., Le Fevre O., Garilli B., Le Brun V., Cassata P., Franzetti P., Maccagni D., Scodeggio M., Zucca E., Zamorani G., Bardelli S., Bolzonella M., Bielby R.M., McCracken H.J., Zanichelli A., Vergani D., Pollo A., 2011, ArXiv 1109.1005

de Lapparent V., 2003, AAP, 408, 845

de Lapparent V., Arnouts S., Galaz G., Bardelli S., 2004, AAP, 422, 841

De Lucia, G., Springel, V., White, S.D.M., Croton, D., Kauffmann, G., 2006, MNRAS, 366, 499

Elbaz D., Dickinson M., Hwang H.S., Díaz-Santos T., Magdis G., Magnelli B., Le Borgne D., Galliano F., Pannella M., Chanial P., Armus L., Charmandaris V., Daddi E., Aussel H., Popesso P., Kartaltepe J., Altieri B., Valtchanov I., Coia D., Dannerbauer H., Dasyra K., Leiton R., Mazzarella J., Alexander D.M., Buat V., Burgarella D., Chary R.R., Gilli R., Ivison R.J., Juneau S., Le Floc'h E., Lutz D., Morrison G.E., Mullaney J.R., Murphy E., Pope A., Scott D., Brodwin M., Calzetti D., Cesarsky C., Charlot S., Dole H., Eisenhardt P., Ferguson H.C., Förster Schreiber N., Frayer D., Giavalisco M., Huynh M., Koekemoer A.M., Papovich C., Reddy N., Surace C., Teplitz H., Yun M.S., Wilson G., 2011, A&A 533, 119

Giavalisco M., Dickinson M., Ferguson H.C., Ravindranath S., Kretchmer C., Moustakas L.A., Madau P., Fall S.M., Gardner J.P., Livio M., Papovich C., Renzini A., Spinrad H., Stern D., Riess A., 2004, ApJL, 600, L103

Greggio L., Renzini A., 1983, AAP, 118, 217

Hogg D.W., Cohen J.G., Blandford R., Pahre M.A., 1998, ApJ, 504, 622

Hopkins A.M., 2004, ApJ, 615, 209

Hopkins A.M., Beacom J.F., 2006, ApJ, 651, 142

Ishida E.E.O., de Souza R.S., Ferrara A., 2011, arXiv, 1106.1745

Jablonka P., Martin P., Arimoto N., 1996, AJ, 112, 1415

Jimenez R., Padoan P., Matteucci F., Heavens A.F., 1998, MNRAS 299, 123

Kennicutt Jr. R.-C., 1998, ApJ, 498,541

Kulkarni V.P., Fall S.M., 2002, ApJ, 580, 732

Kurucz R.L., 1992, IAU Symposia, 149, 225

Larson R.B., 1974, MNRAS, 166, 585

Larson R.B., 1976, MNRAS, 176, 31

Li L.-X., 2008, MNRAS, 388, 1487

Lilly S.J., Le Fevre O., Hammer F., Crampton D., 1996, ApJL, 460, L1

Lilly S., Schade D., Ellis R., Le Fevre O., Brinchmann J., Tresse L., Abraham R., Hammer F., Crampton D., Colless M., Glazebrook K., Mallen-Ornelas G., Broadhurst T., 1998, ApJ, 500, 75

Lin L., Patton D.R., Koo C.D., Casteels K., Hsieh B.C., 2008, *Astronomical Society of the Pacific Conference Series*, 399, 298

Ly C., Malkan M.A., Kashikawa N., Shimasaku K., Doi M., Nagao T., Iye M., Kodama T., Morokuma T., Motohara K., 2007, ApJ, 657, 738

Ly C., Lee J.C., Dale D.A., Momcheva I., Salim S., Staudaher S., Moore C.A., Finn R., 2011, ApJ, 726, 109

Kistler M.D., Yüksel H., Beacom J.F., Hopkins A.M., Wyithe J.S.B., 2009, ApJL, 705, L104

Madau P., Pozzetti L., Dickinson M., 1998, ApJ, 498, 106

Marzke R.O., da Costa L.N., Pellegrini P.S., Willmer C.N.A., Geller M.J., 1998, ApJ, 502, 617

Matteucci F., 1994, AAP, 288, 57

Matteucci F., 2001, Astrophysics and Space Science Library, 253

Matteucci F., Ponzone R., Gibson B.K., 1998, AAP, 335, 855

Matteucci F., Francois, P., 1989, MNRAS, 239, 885

Matteucci F., Greggio L., 1986, AAP, 154, 279

Matteucci F., Tornambé A., 1987, AAP, 185, 51

Menci N., Cavaliere A., Fontana A., Giallongo E., Poli F., Vittorini V., 2004, ApJ, 604, 12

Mobasher B., Dickinson M., Ferguson H.C., Giavalisco M., Wiklind T., Stark D., Ellis R.S., Fall S.M., Grogin N.A., Moustakas L.A., Panagia N., Sosey M., Stiavelli M., Bergeron E., Casertano S., Ingraham P., Koekemoer A., Labbé I., Livio M., Rodgers B., Scarlata C., Vernet J., Renzini A., Rosati P., Kuntschner H., Kümmel M., Walsh J.R., Chary R., Eisenhardt P., Pirzkal N., Stern D., 2005, ApJ, 635, 832

Naab T., Burkert A., 2003, ApJ, 597, 893

Pipino A., Matteucci F., 2004, MNRAS, 347, 968

Pipino A., Matteucci F., 2008, AAP, 486, 763

Pipino A., Devriendt J.E.G., Thomas D., Silk J., Kaviraj, S., 2009, AAP, 505, 1075

Porciani C., Madau P., 2001, ApJ, 548, 522

Reddy N.A., Steidel C.C., 2009, ApJ, 692 778

Rodighiero G., Daddi E., Baronchelli I., Cimatti A., Renzini A., Aussel H., Popesso P., Lutz D., Andreani P., Berta S., Cava A., Elbaz D., Feltre A., Fontana A., Förster Schreiber N.M., Franceschini A., Genzel R., Grazian A., Gruppioni C., Ilbert O., Le Floch E., Magdis G., Magliocchetti M., Magnelli B., Maiolino R., McCracken H., Nordon R., Poglitsch A., Santini P., Pozzi F., Riguccini L., Tacconi L.J., Wuyts S., Zamorani G., 2011, ApJL 739, 40

Salpeter E.E., 1955, ApJ, 121, 161

Seymour N., Dwelly T., Moss D., McHardy I., Zoghbi A., Rieke G., Page M., Hopkins A., Loaring N., 2008, MNRAS 386, 1695

Schechter P., 1976, ApJ, 203, 197

Silva L., Granato G.L., Bressan A., Danese L., 1998, ApJ, 509, 103

Steidel C.C., Adelberger K.L., Giavalisco M., Dickinson M., Pettini M., 1999, ApJ, 519, 1

Strolger L.G., Riess A.G., Dahlen T., Livio M., Panagia N., Challis P., Tonry J.L., Filippenko A.V., Chornock R., Ferguson H., Koekemoer A., Mobasher B., Dickinson M., Giavalisco M., Casertano S., Hook R., Blondin S., Leibundgut B., Nonino M., Rosati P., Spinrad H., Steidel C.C., Stern D., Garnavich P.M., Matheson T., Grogin N., Hornschemeier A., Kretchmer C., Laidler V.G., Lee K., Lucas R., de Mello D., Moustakas L.A., Ravindranath S., Richardson M., Taylor E., 2004, ApJ, 613, 200

Talbot Jr. R.J., Arnett W.D., 1973, ApJ, 186, 51

Takahashi M.I., Shioya Y., Taniguchi Y., Murayama T., Ajiki M., Sasaki S.S., Koizumi O., Nagao T., Scoville N.Z., Mobasher B., Aussel H., Capak P., Carilli C., Ellis R.S., Garilli B., Giavalisco M., Guzzo L., Hasinger G., Impey C., Kitzbichler M.G., Koekemoer A., Le Fèvre O., Lilly S.J., Maccagni D., Renzini A., Rich M., Sanders D.B., Schinnerer E., Scodeggio M., Shopbell P., Smolčić V., Tribiano S., Ideue Y., Mihara S., 2007, ApJS 172, 456

Thomas D., Maraston C., Bender R., 2002, Ap&SS, 281, 371

Tinsley B.M., Danly M., 1976, ApJ, 242, 435

Toomre A., Toomre J., 1976, ApJ, 178, 623

Totani T., Yoshii Y., 1998, ApJL, 501, L177

van de Voort F., Schaye J., Booth C.M., Dalla Vecchia C., 2011, MNRAS, 415, 2782

Vanzella E., Cristiani S., Dickinson M., Giavalisco M., Kuntschner H., Haase J., Nonino M., Rosati P., Cesarsky C., Ferguson H.C., Fosbury R.A.E., Grazian A., Moustakas L.A., Rettura A., Popesso P., Renzini A., Stern D., and GOODS Team, 2008, AAP, 478, 83

White S.D.M., Rees M.J., 1978, MNRAS, 183, 341

Wilson G., Cowie L.L., Barger A.J., Burke D.J., 2002, AJ, 124, 1258